Catalytic potential of CuFe2O4/GO for activation of peroxymonosulfate in metronidazole degradation: study of mechanisms

Article *in* Journal of Environmental Health Science and Engineering · September 2020

DOI: 10.1007/s40201-020-00518-4

CITATION
1

READS
65

4 authors, including:

Mitra Gholami
Iran University of Medical Sciences
192 PUBLICATIONS **1,830** CITATIONS
SEE PROFILE

Mahdi Farzadkia
Iran University of Medical Sciences
220 PUBLICATIONS **2,363** CITATIONS
SEE PROFILE

Ahmad Jonidi jafari
Iran University of Medical Sciences
283 PUBLICATIONS **2,741** CITATIONS
SEE PROFILE

Catalytic potential of $CuFe_2O_4$/GO for activation of peroxymonosulfate in metronidazole degradation: study of mechanisms

Roghayeh Noroozi, Mitra Gholami, Mahdi Farzadkia & Ahmad Jonidi Jafari

Journal of Environmental Health Science and Engineering

e-ISSN 2052-336X

J Environ Health Sci Engineer
DOI 10.1007/s40201-020-00518-4

Springer

Journal of Environmental Health Science and Engineering
https://doi.org/10.1007/s40201-020-00518-4

RESEARCH ARTICLE

Catalytic potential of $CuFe_2O_4$/GO for activation of peroxymonosulfate in metronidazole degradation: study of mechanisms

Roghayeh Noroozi[1] · Mitra Gholami[2,1] · Mahdi Farzadkia[2,1] · Ahmad Jonidi Jafari[2,1]

Received: 27 May 2020 / Accepted: 3 August 2020

Abstract

Application of magnetite nanoparticles ($CuFe_2O_4$/GO) were anchored on graphene oxide (GO), as a Heterogeneous nanocomposite for activating of peroxymonosulfate (PMS) into Metronidazole (MNZ) destruction. The effect of solution pH, reaction time, effectiveness of water matrix components and trapping factors, different catalyst concentrations, PMS and contaminants were evaluated as operating factors on the efficiency of MNZ degradation. Also, mineralization, stability, reactivity and Recycling tests of the catalyst, and the degradation kinetics were performed. MNZ degradation and mineralization were obtained under optimal conditions (0.2 g/L catalyst, pH = 5, 30 mg/L MNZ and 2 mM PMS), 100% and 41.02%, respectively over 120 min. Leaching of Fe and Cu was found <0.2 mg/L for $CuFe_2O_4$/GO showed a high stability of catalyst, and a significant recyclability was achieved $CuFe_2O_4$/GO within 5 times consecutive use. MNZ degradation affected by anions was reduced as follows: $HCO_3^- > NO_3^- > Cl^- > SO_4^{2-}$. The experimental data were very good agreement with pseudo-first-order kinetic model, and during quenching tests $SO_4^{\bullet-}$ radicals played a dominant role in the degradation process of MNZ. As a result, the CuFe2O4/GO/PMS system can be described as a promising activation of PMS in MNZ degradation, due to its high stability, reusability and good catalyst reactivity, and the production of reactive species simultaneously.

Keywords Metronidazole · $CuFe_2O_4$ · Peroxymonosulfate · Graphene oxide

Introduction

The use of antibiotics in the pharmaceutical manufacturing and household and hospitals applications has increased in recent decades. Today, drug substances have been traced in the effluents of wastewater treatment plants, groundwater, surface water, and drinking water [1–4].

Antibiotics are resistant organic substances that have adverse effects on environment and human health, and their release, even at low concentrations, causes bacterial resistance [2, 5–7].

Metronidazole (MNZ) is one of the most common nitroimidazole antibiotics used to treat infectious diseases caused by protozoa and anaerobic bacteria, in both humans and animals. Also, MNZ is added as anti-parasitic agent to fish and chicken feeds in veterinary medicine [8–10].

The mutagenicity of this antibiotic in humans and its carcinogenicity in animals have been investigated and confirmed. [11]. Due to the biological stability and high solubility in water, the use of advanced technologies to remove these antibiotics has been considered [9, 11]. Many methods such as surface adsorption [11, 12], optical decomposition [8, 13], chemical oxidation [14], electrochemical degradation [15, 16], and biological decomposition [17] have been used to remove the MNZ antibiotic, And disadvantages such as the production of toxic by-products, excess sludge, the need for additional treatments, low efficiency, and investment costs for most of these technologies have been reported [2, 9]. Advanced oxidation processes (AOPs) have been considered as effective processes in mineralization, reducing toxicity and improving the biodegradability of resistant contaminants [2, 18–20]. One of the AOPs processes that have been introduced

✉ Mitra Gholami
gholamim@iums.ac.ir; gholamimitra32@gmail.com

[1] Department of Environmental Health Engineering, Iran University of Medical Sciences, Tehran, Iran

[2] Research Center for Environmental Health Technology, Iran University of Medical Sciences, Tehran, Iran

Published online: 07 September 2020

as a desirable process in recent years, is the production of sulfate ($SO_4^{\bullet-}$) and hydroxyl ($^{\bullet}OH$) free radicals. The $SO_4^{\bullet-}$ radical has a high chemical oxidation potential ($SO_4^{\bullet-}$, 2.5–3.1 V and $^{\bullet}OH$, 1.8–2.7 V), and is capable of mineralizing many resistance contaminants [18, 21, 22]. Elimination of pollutants by AOPs processes is based on the production of hydroxyl ($^{\bullet}OH$) and sulfate ($SO_4^{\bullet-}$) free radicals [18]. $SO_4^{\bullet-}$ radicals have a higher reactivity than $^{\bullet}OH$ radicals. These radicals are produced through chemical or photochemical reactions.$SO_4^{\bullet-}$ radicals are produced by activating peroxymonosulfate (PMS). There are several methods to activate PMS, such as chemical and photochemical reactions (2). According to previous studies, the performance of metal heterogeneous catalysts, especially transition metals (Ag^{+}, Ni^{2+},Co^{2+}, Fe^{2+}, Cu^{+2}, Fe^{3+}, Mn^{2+},Ce^{3+}, etc.), have been favorable for activating PMS [23, 24]. Metal ions-based heterogeneous catalysts, in comparison with homogeneous ones (H_2O_2/Fe^{2+}, H2O2 /Fe2+/UV [25], electro/Fe^{2+}/PS [26], etc.), can effectively overcome the difficulties in reusability, and prevent from secondary pollution associated with leaching of transition metals due to the stable physico chemical structure [27]. Magnetizing of heterogeneous catalysts is an effective and cost-effective method to solve their separation problems from solution samples [27]. Hence, magnetic nanoparticles (MNPs) M^{2+} Fe_2O_4 (M = Zn, Cu, Mn, Co, etc.) showed high efficiency in activating PMS and producing $SO_4^{\bullet-}$ radicals [23]. Agglomeration of $CuFe_2O_4$ MNPs and low surface activity reduces the rate of degradation, so, to overcome this problem and increase the rate of catalytic reactions, $CuFe_2O_4$ MNPs are coated on supporting substances such as activated carbon, chitosan, zeolite and polymer [2, 27]. Graphene oxide (GO) is a two-dimensional nanocatalyst with great surface area and a good hydrophobic for use in aqueous solutions. GO has been used in heterogeneous catalysis application as a support for nanoparticles in pollutant degradation, and due to the great adsorption capacity, chemical and physical stability, high electrical conductivity can enhances performance of MNPs in oxidation of pollutant [2, 28].

Although the oxidation of MNZ by various catalysts has been studied by other researchers [8, 13, 29], no research has been done on the activation of PMS by $CuFe_2O_4$ MNPs for degradation of MNZ. Also, $CuFe_2O_4$ MNPs supported on graphene oxide can increase the efficiency of nanoparticles in the degradation of MNZ. The aim of this study was to investigate the specifications and application of $CuFe_2O_4$ MNPs in activation of PMS for MNZ degradation and there is no published article on MNZ degradation by $CuFe_2O_4$/GO system. Also, in the study, the effect of key factors in efficient degradation of MNZ Such as contact time, several concentration of catalyst, PMS and pollutant, solution pH, the reusability, stability and mineralization degree and kinetics of the process were all investigated.

Materials and methods

Materials

All chemicals and powders were used with high purity and without extra modification or purification. Acetonitrile with HPLC grade, $KMnO_4$, $NaNO_3$, NaHCO3, Na_2SO_4, NaCl were provided from Merck Co. ferric nitrate nonahydrate ($Fe(NO_3)_3 \cdot 9H_2O > 99\%$), copper nitrate trihydrate ($Cu(NO_3)_2 \cdot 3H_2O$ 99%), methanol (MeOH), tert-butyl alcohol (TBA), Peroxymonosulfate ($KHSO_5 \cdot 0.5KHSO_4 \cdot 0.5K_2SO_4$, oxone®(,ethanol, graphite powder (> 99.5% purity with <45 μm) and MNZ were provided from Sigma Aldrich Chemical Co. magnet with intensity 1.5 T used to separate catalysts from the solution.

Synthesis of $CuFe_2O_4$/GO

Graphene oxide NPs were prepared using of the modified Hummer's method [30]. To synthesize the $CuFe_2O_4$/GO composite, first 2 g of the synthesized GO was added to 100 ml of distilled water and placed in an ultrasonic bath for 2 h. then, GO sonicated added to a 500 ml flask containing a mixture of 10 ml (0.025 M) Cu $(NO_3)_2 \cdot 3H_2O$ and 20 ml (0.05 M) of Fe $(NO_3)_3 \cdot 9H_2O$ and mixture was stirred at room temperature for 15 min using a mechanical mixer, and pH mixture adjusted at 12 using of solution 2 M NaOH in a drop wise state and a dark solution was obtained. Then, the mixture was stirred again for 2 h at 90 °C. After cooling, solid product separate from solution by a magnet and washed with ethanol and distilled water and then dried at 80 °C for 2 h by oven and calcined at 700 °C for 5 h in a furnace [2].

Characterization and analytical methods

As can be seen in Table 1, describe the physic-chemical, textural, morphological and magnetic properties using of various instruments (i.e., XRD, FESEM, EDX, BET, TEM, and VSM) were applied.

Analytical methods

Residual concentration of MNZ was detected by HPLC (Shimadzu LC-20) with ultraviolet detector and C18 column (250 × 4.6 mm^2, 5 μm, USA). The wavelength of 318 nm was set for the UV detector and the column operating temperature was kept at 25°C. The mobile phase contained ratio of 20:80 (*v*/v %) acetonitrile and water in flow rate of 1.0 mL/min. Analyze of Total Organic Carbon (TOC) was performed by TOC analyzer (Analytik Jena AG Corporation, 2100). atomic absorption spectrophotometer (AA-7000, **Shimadzu**) was use for detect of Fe and Cu leached.

Table 1 Details about instruments used to properties of samples

Method	Equipment type	Application
XRD[a]	Philips, PW1730, Netherlands	To X-ray powder diffraction pattern of various samples.
FESEM[b]	FESEM,Mira 3- XMU	To morphology properties evaluate of GO, $CuFe_2O_4$, $CuFe_2O_4$/GO.
TEM[c]	Philips, EM, Netherlands	To analysis the size and shape of nanoparticles.
EDS[d]	Mira 3- XMU	For elemental analysis of $CuFe_2O_4$/GO.
BET[e]	Quantochrome, NOVA 2000,USA	To textural feature analysis of different samples.
VSM[f]	7400, Lake Shore, USA	To evaluation the magnetic properties of samples.

[a] X-ray diffraction

[b] Field emission scanning electron microscope

[c] transmission electron microscope

[d] energy dispersive X-ray spectrometer

[e] Brunaeuer–Emmett–Teller

[f] vibrating sample magnetometer

Adsorption studies

Initially, a specific dose of catalyst was added to the MNZ solution with a specific concentration and pre-adjusted pH. The sample was placed on a mixer with a speed of 250 rpm to achieve an adsorption/desorption equilibrium. Then, at different times (0–180 min), 2 ml of the sample was taken from the solution after catalyst separation magnetically by a magnet. Sample filtered with a 0.22 μm syringe filter, and then injected into HPLC to determine the remaining antibiotic concentration. Adsorption kinetic studies were performed using optimal pH and 30 mg/L concentration of MNZ and 0.2 g/L adsorbent dose, and for adsorption isotherm different were used concentrations of MNZ and different adsorbent doses at optimal pH.

The catalytic degradation and optimization procedure

At each stage of the experiment, after equilibrium time (60 min), the catalytic destruction reactions of the MNZ was started by adding a certain amount of PMS and catalyst into reactor contain solutions with adjusted pH of 5. During the reaction, the samples were mixed with a mixer (250 rpm). Then, at different times (60–120 min), 2 ml of the sample was taken from the solution after catalyst separation magnetically by a magnet and the MNZ remaining concentration determined by HPLC. The degradation efficiency (%) was obtained using Eq. (1). Under above operating conditions, catalytic process of MNZ was optimized at different experimental parameters such as solution pH, various doses of catalyst, PMS, pollutant over 120 min reactions. After optimization, the following tests were investigated as: the effect scavengers such as ethanol (EtOH) and tert-butanol (TBA), the effect of co-existing water matrix such as: HCO_3^-, NO_3^-, Cl^- and SO_4^{2-}, efficiency $CuFe_2O_4$/GO/PMS system in degradation of MNZ for five consecutive runs and finally a possible mechanism was suggested for the PMS activation and production of reactive oxidizing species for catalytic degradation of MNZ.

$$\text{Removal rate} = \left(1-\frac{C_t}{C_0}\right) \times 100\% \quad (1)$$

C_0 and C_t the primary and residual concentrations of MNZ (mg/L), respectively.

Results and discussion

Characterization of $CuFe_2O_4$/GO

As shown in Fig. 1a, the XRD peaks for $CuFe_2O_4$ MNPs appear at angles 2θ =18.50°, 30. 20°, 35.80°, 43.05°, 57.05° and 62.80° correspond to the standard card number 25–0283, which is consistent with the Joint Committee on Powder Dispersion Standards (JCPDS) [2]. The angle of the $CuFe_2O_4$ peaks in the $CuFe_2O_4$/GO catalyst has been maintained without any change, indicating that the $CuFe_2O_4$ MNPs are well coated on GO. The specified peaks assigned to GO at 2θ value 10.2, but no specific peaks of GO can be seen in $CuFe_2O_4$/GO composite, which can be due to the production and growth of $CuFe_2O_4$ MNPs on GO surface and the disappearance of peaks related to GO [2]. Structural analysis of XRD and its comparison with the standard sample model indicate that the catalyst is well synthesized with high purity. The EDS spectroscopy for the $CuFe_2O_4$/GO is shown in Fig. 1b. Peaks prove the presence of Fe, Cu, O and C in the composite structure. The weight percentage of each atom was calculated as follows: Fe = 34.49%, Cu = 24.59%, O =

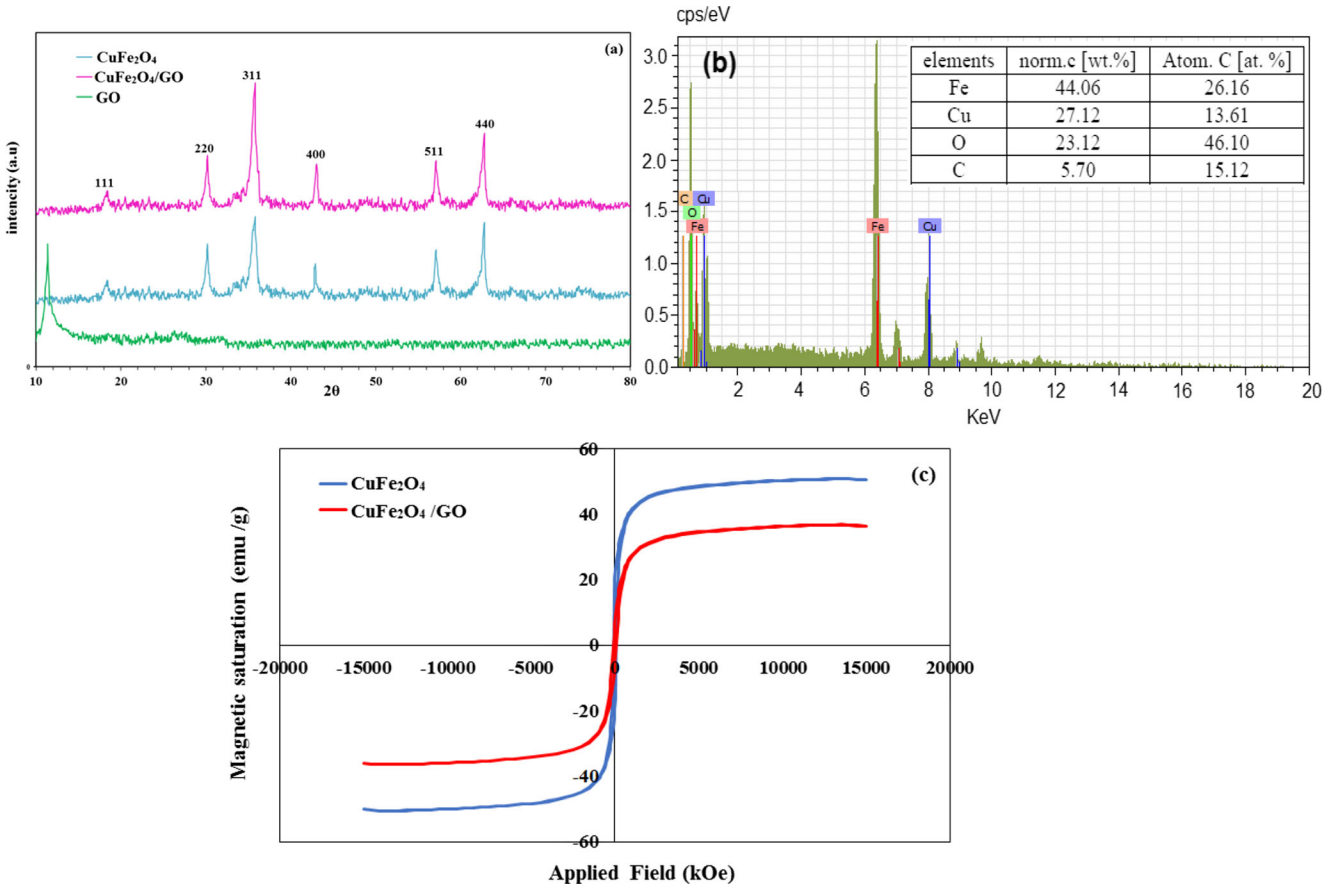

Fig. 1 XRD patterns of GO, $CuFe_2O_4$ and $CuFe_2O_4$/GO (**a**), EDS spectrum of $CuFe_2O_4$/GO (**b**) and hysteresis loops of $CuFe_2O_4$ and $CuFe_2O_4$/GO (**c**)

30.60% % and C = 10.31%. The position of the peaks indicates that the $CuFe_2O_4$/GO has been synthesized with high purity. The uniform distribution of each component can indicate that all the primary components have entered the crystal lattice during the synthesis process. Also, the result of EDS analysis showed that the atomic proportion of iron to copper was 1:1.69. Figure 1c shows the VSM analysis and the magnetic hysteresis loops related to $CuFe_2O_4$ and $CuFe_2O_4$/GO samples. The highest magnetization saturation (MS) for $CuFe_2O_4$/GO and $CuFe_2O_4$ were obtained 36.76 and 50.74 emu/g. Low MS for $CuFe_2O_4$/GO composite compared to $CuFe_2O_4$ is due to the non-magnetic presence of GO in the $CuFe_2O_4$/GO structure [31, 32]. The catalyst showed good magnetic properties in a magnetic field; therefore, it can be used as a reusable catalyst in real applications due to its rapid separation and prevention of environmental pollution. The TEM image of the $CuFe_2O_4$/GO composite in Fig. 2a confirms $CuFe_2O_4$ nanoparticles are well with a uniform distribution And low accumulation (dark spots) coated on layer of GO sheets (white dots), and The TEM image with magnifications of 100 nm shows composite particles diameter approximately 30 nm. Images of FESEM analysis of GO, $CuFe_2O_4$ and $CuFe_2O_4$/GO are shown in Fig. 2b-d. GO NPs are visible with a layered structure and recognizable edges of the sheets (Fig. 2b). A typical spherical with size between 33 to 40 and 30 to 38 nm is observed for $CuFe_2O_4$ MNPs and $CuFe_2O_4$/GO catalysts, respectively (Fig. 2(c and d)). Comparison of $CuFe_2O_4$ MNPs with $CuFe_2O_4$/GO composite shows that the outer surface of $CuFe_2O_4$/GO is very porous and with low accumulation of particles, which can increase additional active sites and increase catalytic activity during oxidation reactions.

The results of $CuFe_2O_4$/GO catalyst analysis by adsorption-and-adsorption of N_2 at $77^{\bullet K}$ showed that according to the IUPAC classification, the isotherm form is of type IV and is related to porous structures the size of mesoporous cavities. According to the results of the BET specific surface area (S_{BET}) analysis, the specific surface area of the $CuFe_2O_4$/GO, $CuFe_2O_4$ and GO was 46.78, 34.66 and 113.80 s m^2/g, respectively, and the total pore volume and pore size distributions (According Barrett–Joyner–Halenda (BJH) analyses) to of the GO, $CuFe_2O_4$ and $CuFe_2O_4$/GO was 0.0853, 0.093 and 0.107 cm^3/g nm and 3, 9.2 and 10.73 nm respectively (Table 2). The results of the BET analysis are consistent with the results of studies conducted in this field [33, 34]. The decrease in GO specific surface area is due to the entry of $CuFe_2O_4$ MNPs into the GO structure and the filling of the space inside the cavities by it.

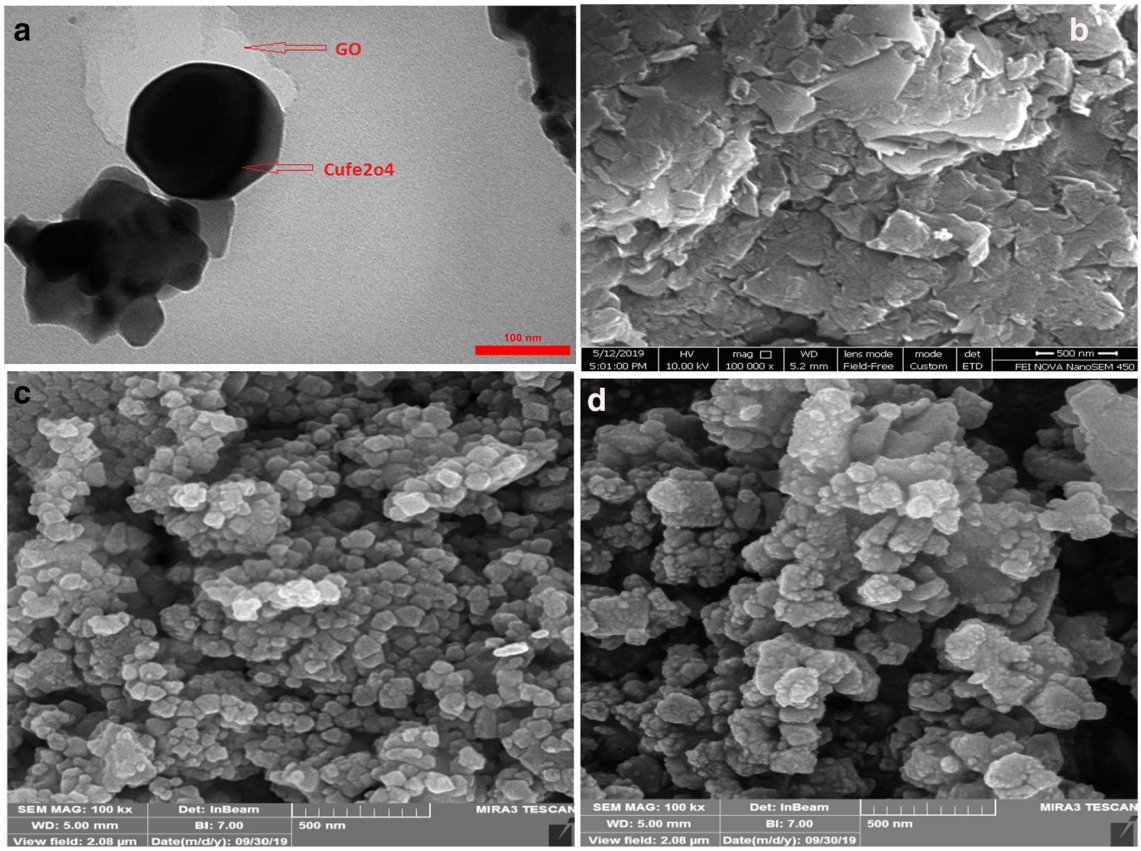

Fig. 2 TEM image of $CuFe_2O_4$/GO (**a**), FESEM images of GO (**b**), $CuFe_2O_4$ (**c**) and $CuFe_2O_4$/GO (**d**)

Adsorption equilibrium studies

Adsorption is known as part of heterogeneous catalyst systems. As shown in to Fig. 3(a), in the first 30 min, the curve has a steep slope and the adsorption capacity has increased rapidly, possibly due to the large number of active and unsaturated sites on adsorbent surface. After 60 min, there were no significant changes in the adsorption of MNZ on the $CuFe_2O_4$/GO, Which can be caused by the filling of active sites on the adsorbent surface or the completion of the adsorption capacity [35]. As a result, 60 min was chosen as the equilibrium time.

The pseudo-first-order (PFO) and pseudo second order (PSO) models were used to study the kinetics of adsorption, and the values of the kinetic parameters of the MNZ adsorption process on $CuFe_2O_4$/GO are shown in Table 3. The results showed that the $q_{e,cal}$ compared to the $q_{e,ex}$ in the PSO model is more than the PFO model, and also according to the regression coefficient obtained $R^2 = 0.98$ (Fig. 3(a) inset), it was found that the adsorption process follows the second-order kinetic model. Freundlich and Langmuir isotherms were used to evaluate the adsorption behavior of MNZ molecules on f $CuFe_2O_4$/GO. Adsorption tests were performed for different concentrations of adsorbent (0.05 to 0.6 g/L) and the results are presented in Table 3. The results of experimental data showed that the regression coefficient of Langmuir isotherm is higher than that of isotherm Frondelich; therefore, the Langmuir isotherm model is more suitable for adsorption MNZ on $CuFe_2O_4$/GO. The Langmuir isotherm model shows that the adsorption of MNZ on the $CuFe_2O_4$/GO is single-layered and the surface of the adsorbent has limited and identical absorption sites, in accordance with the literature [31, 36–38].The findings also showed that with increasing the adsorbent dose from 0.05 to 0.6 g/L, the maximum adsorption capacity (q_m) increased from 8.92 to 46.29 mg/g, which is due to the increase adsorption surface and increase access of adsorbent molecules on the adsorbent surface [35, 39, 40].

Table 2 Texture properties of GO, $CuFe_2O_4$, and $CuFe_2O_4$ /GO

Samples	SBET $m^2\ g^{-1}$	V_{meso} $cm^3\ g^{-1}$	D_{meso} nm	Pore structure
GO	113.80	0.0853	3	Mesopore
$CuFe_2O_4$	34.66	0.093	10.73	Mesopore
$CuFe_2O_4$ /GO	46.78	0.107	9.2	Mesopore

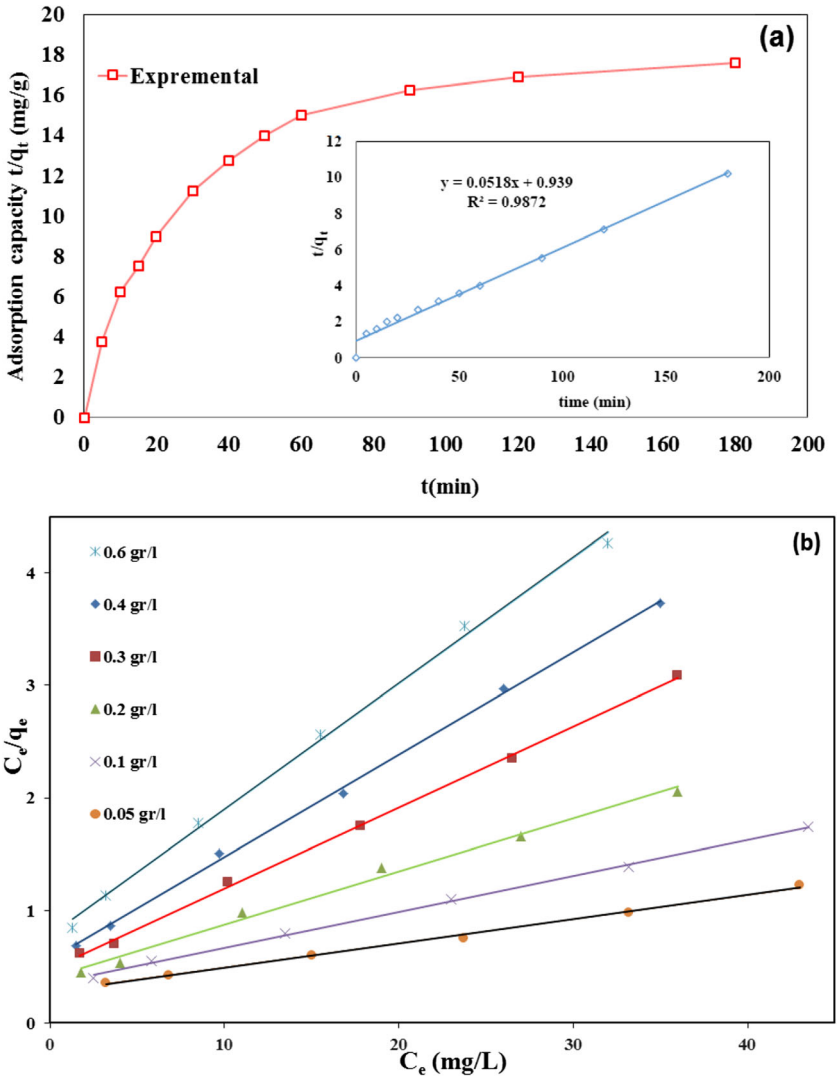

Fig. 3 equilibrium adsorption capacity and pseudo-second- order model (inset) (**a**), liner Langmuir isotherm model (**b**) for MNZ adsorption on $CuFe_2O_4$/GO (pH: 5, T: 25 ± 1 °C), (**a**) MNZ: 30 mg/L, $CuFe_2O_4$/GO: 0.2 g/L and contact time: 180 min; (**b**) MNZ: 5–50 mg/L, $CuFe_2O_4$/GO: 0.05–0.6 g/L and contact time: 60 min)

Comparison of different processes in MNZ removal

In order to determine the effectiveness of the catalyst, the efficiency of its process can be compared with different processes in degradation of MNZ under same operating conditions.

The finding of Fig. 4 shows that the lowest removal efficiency is related to PMS (15%), CuFe2O4 (20%) and GO (25.2%) alone, indicating that each of these processes alone does not have sufficient potential to degradation MNZ. Also, an increase in the efficiency of removal with the presence of $CuFe_2O_4$/GO (36.60%) can be associated with an increase in active sites available for adsorption of MNZ molecules. According to the results, the elimination efficiency has increased when PMS and $CuFe_2O_4$ or PMS and $CuFe_2O_4$/GO have been used together. The reason for the increase in efficiency $CuFe_2O_4$/PMS (77%)and $CuFe_2O_4$/GO/PMS(%100) during 60 min compared to other processes is due to the decomposition of PMS molecule and production of active $SO_4^{\bullet-}$ radicals, which eventually leads to oxidation reactions and chemical decomposition of MNZ [41]. Therefore, $CuFe_2O_4$/GO/PMS system was selected as the best process in MNZ degradation.

Kinetic analysis

Kinetic models of MNZ degradation in heterogeneous catalyst system were studied, and evaluated models of second, first and zero order for present process. The results showed that the PFO kinetic model had the highest compliance Compared to the other models studied for MNZ degradation by $Cufe_2O_4$/GO/PMS process, and the regression coefficient for PFO model for all the studied parameters was $R^2 > 0.98$. The reaction rate constant (k_{obs}) during 60 for various parameters effective in the destruction of MNZ by $Cufe_2O_4$/GO/PMS system are given in figure inserted in Fig. 5a–d.

Table 3 The values of kinetics and isotherms of MNZ adsorption on $CuFe_2O_4$/GO

Models	Parameters	Value
Kinetic		
Pseudo-first-order	$q_{e,cal}$ (mg/g)	18.50
	k_f (min^{-1})	0.017
	R^2	0.9469
Pseudo-second-order	$q_{e,cal}$ (mg/g)	19.30
	ks (g/mg min)	0.002
	R^2	0.9872
	$q_{e,exp}$ (mg/g)	15
Isotherm		$CuFe_2O_4$ / GO concentration
Freundlich	kF	0.05 0.1 0.2 0.3 0.4 0.6
	(mg/g(L mg)$^{1/n}$)	6.62 4.52 3.66 2.87 2.17 1.62
	n	1.91 2.00 2.09 2.11 2.18 2.21
	R^2	0.9844 0.9871 0.9921 0.994 0.9651 0.9973
Langmuir	q_0 (mg/g)	8.92 10.96 13.88 21.09 31.34 46.29
	k_L (L/mg)	0.16 0.15 0.14 0.11 0.09 0.07
	R^2	0.9971 0.9987 0.999 0.9917 0.9984 0.9961

Effect of operational factors and optimization conditions

The solution pH is one of the effective parameters in the AOPs. It can influence solubility and activity of oxidant, pollutant and catalyst surfaces property, kinetics of reactions and generating free radicals [42]. As shown in Fig. 5a, the effect of the pH on the MNZ degradation in $CuFe_2O_4$/GO/PMS system was evaluated in the range of 3.0–11.0. The results showed that PH had an effect on system performance and complete removal of metronidazole was not achieved for all pH values studied over 120 min, so high efficacy in metronidazole removal was observed under acidic conditions and low efficacy in Alkaline conditions occurred [11, 43]. MNZ removal efficiency and reaction rate constant decreased from %100 and 0.0844 min^{-1} to % 51 and 0.0082 min^{-1} respectively by increasing the pH from 3to11 for 120 min. In acidic pHs, more $SO4^{\bullet-}$ radicals are produced. Also, under acidic conditions, the

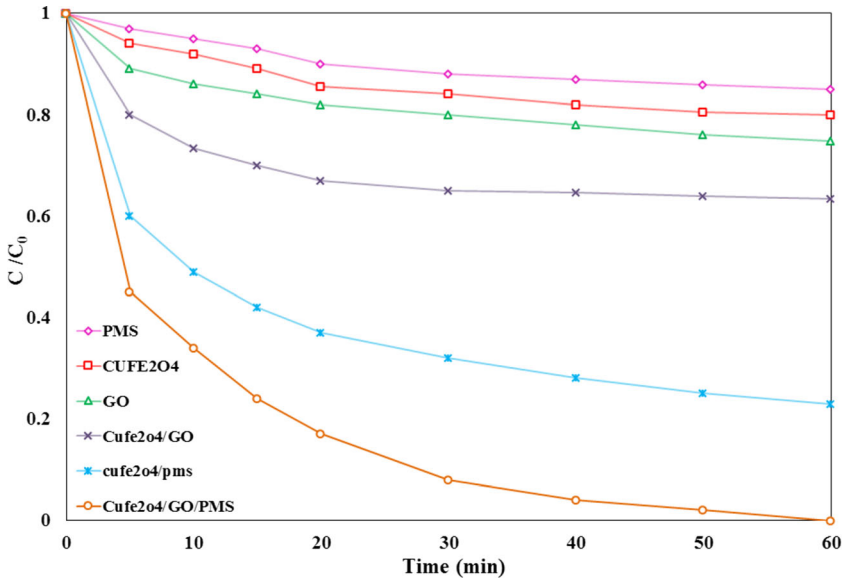

Fig. 4 MNZ removal efficiency with different processes (b) under optimum conditions (pH: 5, MNZ: 30 mg/L, PMS: 2 mM, PMS, $CuFe_2O_4$, $CuFe_2O_4$/GO, GO, $CuFe_2O_4$/PMS and $CuFe_2O_4$/GO/PMS: 0.2 g/L and $T = 25 \pm 1^{\circ}C$)

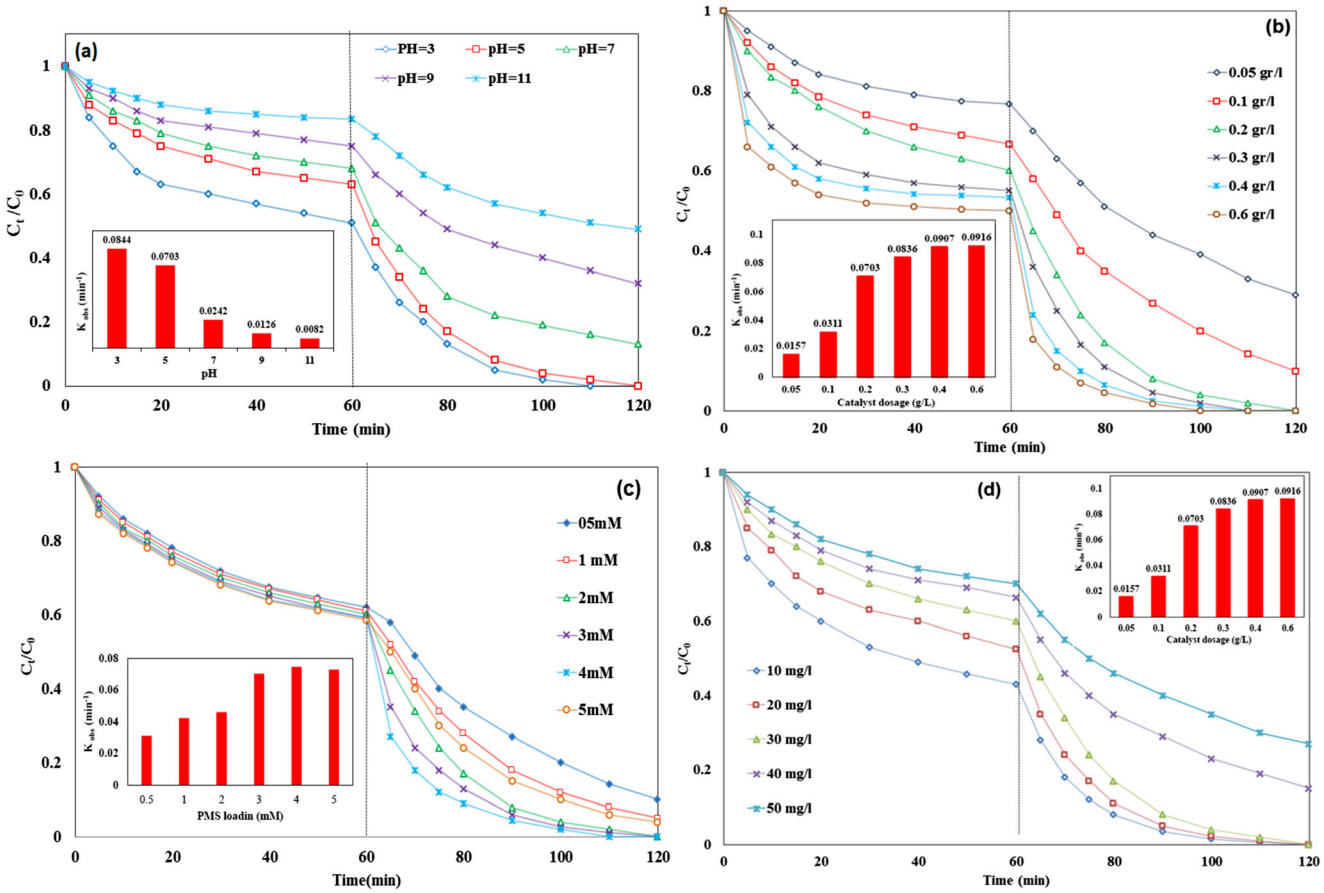

Fig. 5 effect of Factors affecting on the MNZ removal by CuFe2O4/GO/PMS system over 120 min reaction: (**a**) pH; (**b**) catalyst doses (**c**) initial PMS concentration; (**d**) initial MNZ concentration(Experimental condition: temperature 25 ± 1 °C, (a) 0.2 g/L catalyst, 2 mM PMS, 30 mg/L MNZ (b) pH = 5.0, 2 Mm PMS, 30 mg/L MNZ; (c) pH = 5.0, 0.2 g/L catalyst, 30 mg/L MNZ; (d) pH = 5.0, 2 Mm PMS, 0.2 g/L catalyst). The inset displays the MNZ degradation rate at different solution pH (a), dosages of catalyst (b), PMS (c) and at various concentration of MNZ (d)

dissolution of iron ions increases and increases the reaction rate between PMS molecules and iron ions, and more reactive species are produced [44]. Also, the pKa value of MNZ is 2.38 and the measured pH $_{pzc}$ for $CuFe_2O_4$/GO is about 6.95. Therefore, under acidic pH, Metronidazole molecules have a positive charge and the catalyst has a negative charge and there is adsorption force between MNZ and the catalyst. With the increase in PH from 5 to 7, the efficiency of removal was reduced from 100% to 87%, and the removal efficiency of more than 80% indicates the good potential of the catalyst in removing the MNZ. In pH from 5 to 7, Both $SO_4^{\bullet-}$ and $^{\bullet}OH$ radicals are present in system [45].

And the most effective removal was under acidic and natural conditions.

At the alkaline pHs (pH > 9.0), Elimination efficiency decreases for several reasons: i. the alteration of the $SO_4^{\bullet-}$ to $^{\bullet}OH$ radicals and the production of SO_4^{2-} anion, which has low oxidation potential Eq. (2) ii. The increasing production of SO_5^{2-} at conditions of pH >9 as the dominant PMS species and the occurrence of chain reactions in the system as a result of its production Eqs. (3) and (4) [41, 46]. Also, the negative charge of catalytic surface the presence of metronidazole in the form of MNZ-OH^- under alkaline conditions lead to a predominance of repulsion force and a reduction in removal efficiency [12]. The pH value of 5 was chosen for MNZ removal by catalyst as PMS activator.

$$SO_4^{\bullet-} + OH^- \rightarrow SO_4^{2-} + {}^{\bullet}OH \quad (2)$$

$$SO_5^{2-} + H_2O \leftrightarrow HSO_5^- + OH^- \quad (3)$$

$$^{\bullet}OH + SO_5^{2-} \rightarrow SO_5^{\bullet-} + OH^- \quad (4)$$

The dose optimal of catalyst for antibiotic degradation was determined by evaluating doses of 0.05 to 0.6 g/L. in Fig. 5b an increase in degradation efficiency of MNZ and k_{obs} was observed from 71% to 100% and 0.0157 to 0.0916 min^{-1}, when catalyst dosage was increased.

This progress is possible due to the increased activation of PMS and produce more oxidizing species at high doses of the catalyst [41], The results of this study are consistent with

previous reports [28, 41, 47]. Although a complete elimination of MNZ was achieved at a dose of 0.6 g/L in 100 min reaction, dose of 0.2 g/L was selected as the optimal dose economically with a removal efficiency of 100% during 120 min, because, Significant changes were not observed with increasing catalytic dose from 0.2 g/L.

The effect of different concentrations of PMS in the removal efficiency of the MNZ is displayed in Fig. 5c. The results showed, Increase the concentration to a specific dose has a significant effect on metronidazole degradation. k_{obs} increased from 0.0311 to 0.0703 min^{-1} when the PMS concentration increased from 0.5 to 3.0 mM, Then, with increasing concentration to 4 mM Slight changes were observed, and k_{obs} slightly increased to 0.0744 min^{-1}, Then, it is slowly reduced to 0.0728 min^{-1} with increasing concentration PMS to 6.0 mM. Similar results have been observed in various radical sulfate-based processes from previous reports [48, 49].

So, a concentration of 2 mM was determined as the optimum concentration. At low concentrations of PMS, because at the catalyst surface, active sites are not used effectively, the rate of catalytic oxidation reactions and removal efficiency are reduced.

On the other hand, in additional concentrations of PMS, the number of active sites available decreases, resulting in reduced oxidation reactions and removal efficiency, Which could be due to increased production of $SO_4^{\bullet-}$ and $^{\bullet}OH$ radicals [24] could also be related to the effect of quenching PMS (Eqs. (5) and (6)) and the re-combination of $SO_4^{\bullet-}$ and $^{\bullet}OH$ radicals (Eqs. (7) and (8)) and the reaction of radicals to each other and their consumption (Eq. 9) [21].

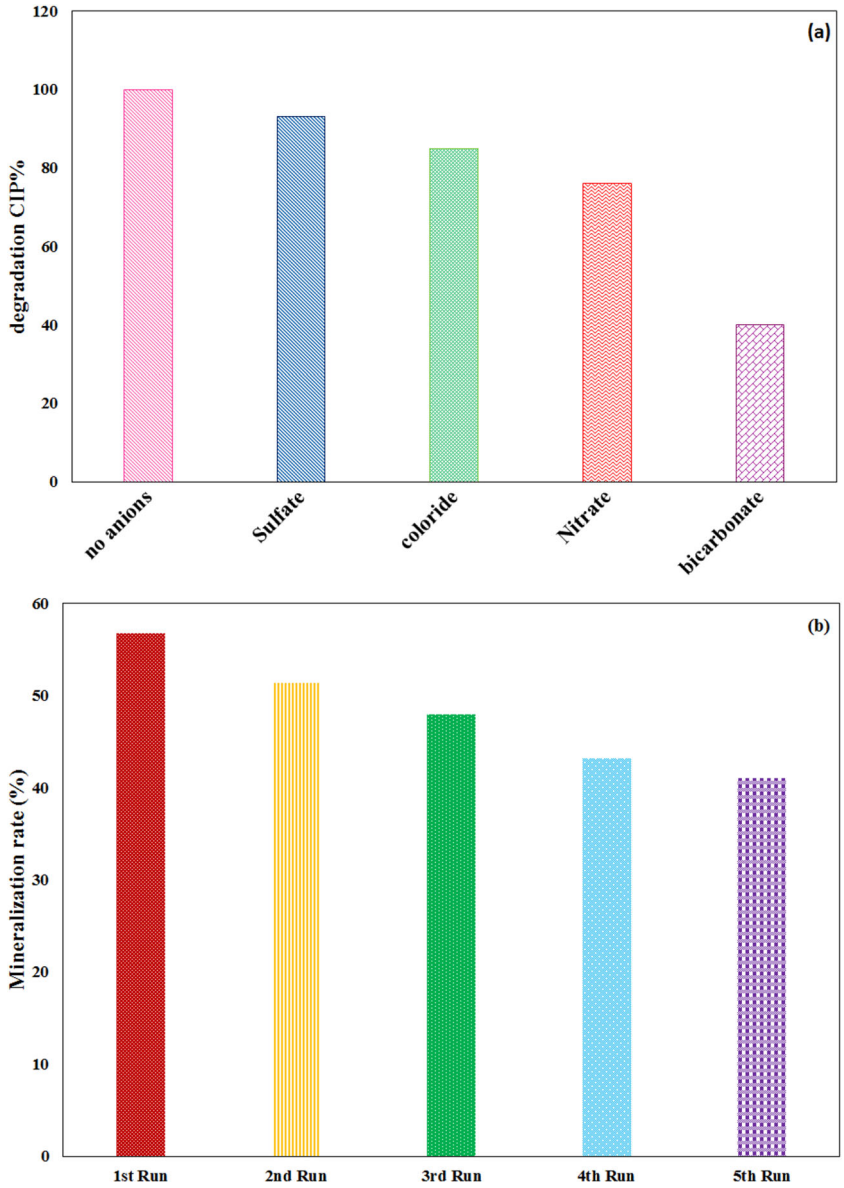

Fig. 6 Effects of 50 Mm inorganic anions on MNZ degradation by $CuFe_2O_4$/GO /PMS system (**a**) and Mineralization of process during several consecutive cycles by $CuFe_2O_4$/GO /PMS system (**b**) at optimized conditions over 60 min reaction

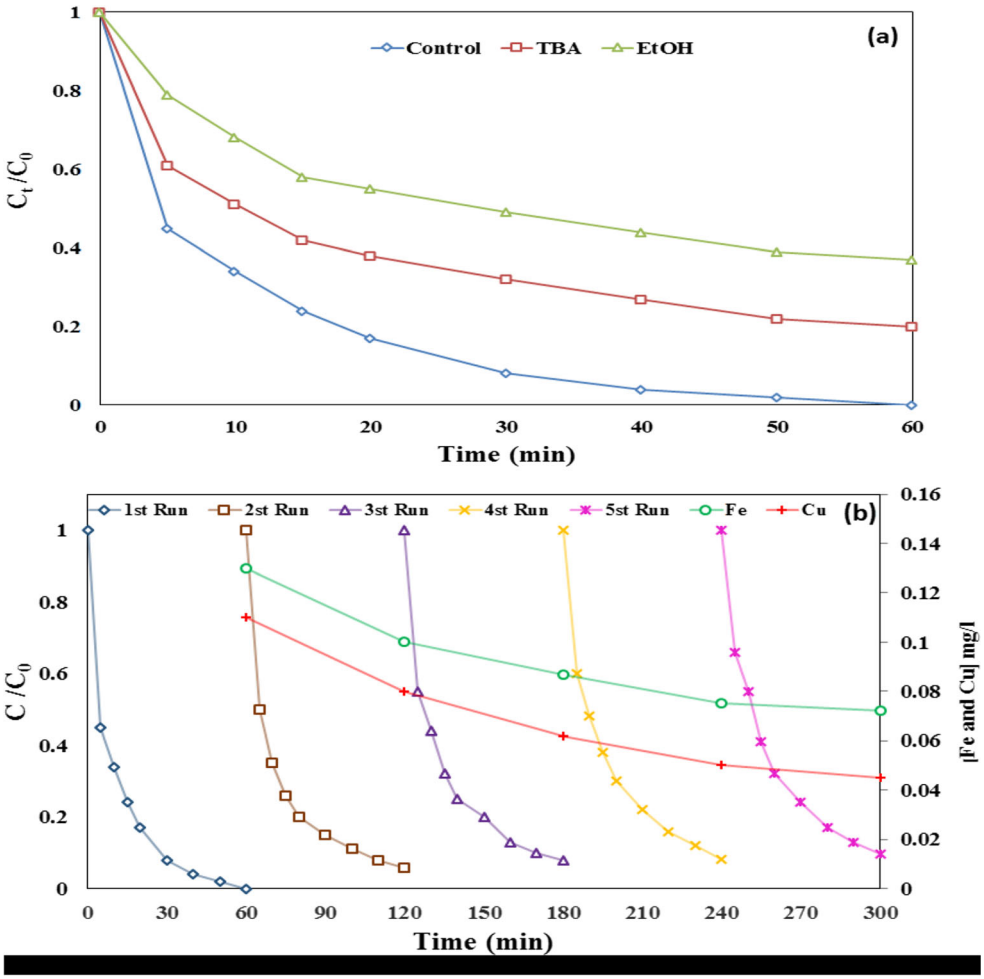

Fig. 7 the effect of 50 mM various quencher on MNZ degradation (**a**) and Reusability and stability of $CuFe_2O_4$/GO for MNZ degradation (**b**) within 60 min reaction (Reaction conditions: pH: 5.0, MNZ: 30 mg/L, PMS: 2 mM, $CuFe_2O_4$/GO: 0.2 g/L)

$$\rightarrow SO_4^{\bullet-} + HSO_5^- \qquad SO_4^{2-} + SO_5^{\bullet-} + H^+ \qquad (5)$$

$$\rightarrow {}^{\bullet}OH + HSO5^- \qquad H_2O + SO_5^{\bullet-} \text{ or } HO_2^{\bullet} + HSO_4^- \qquad (6)$$

$$\rightarrow SO_4^{\bullet-} + SO_4^{\bullet-} \qquad 2SO_4^{2-} \text{ Or } S_2O_8^{2-} \qquad (7)$$

$$\rightarrow {}^{\bullet}OH + {}^{\bullet}OH \qquad H_2O_2 \qquad (8)$$

$${}^{\bullet}OH + \rightarrow SO_4^{\bullet-} \qquad HSO_4^- + \S\, O_2 \qquad (9)$$

Figure 5d shows MNZ removal efficiency and k_{obs} under various concentrations of MNZ over 120 min. As shown, when MNZ concentration changed from 10 to 50 mg/L, the k_{obs} and removal efficiency decreased from 0.0157 min^{-1} to 0.0916 min^{-1} and %100 to 73%. Therefore, the concentration of the pollutant is inversely related to the removal efficiency. Elimination efficiency 100% was obtained for concentrations of 10 to 30 mg/L over 120 min of reaction, while concentrations of 40 and 50 mg/L, a reaction time longer than 120 min was required to achieve complete elimination. The results of this study are similar with other studies on the use of heterogeneous catalysts [2, 48]. The reason for the decrease in catalytic decomposition efficiency with increasing MNZ concentration can be considered as the presence of a certain number of active radicals produced in the solution to react with a fixed number of pollutant molecules [2, 18].

Also, at high concentrations of pollutants, larger amounts of pollutants are adsorbed at the catalyst surface, which leads to a reduction in the contact of the pollutant with the active radicals and thus a reduction in the efficiency of pollutant degradation [2].

The effect of anions

Figure 6a shows that adding 50 mM of anion reduces the efficiency of metronidazole elimination within 60 min under optimal conditions 0.2 g/L catalyst pH 5.0, 30 mg/L MNZ and 2 mM PMS. The reduction in MNZ removal in the presence of various anions was $HCO_3^- > NO_3^- > Cl^- > SO_4^{2-}$. The reduction in the efficiency of the main pollutant in the presence of interfering agents in the form of anions can be attributed to the following reasons: Anions react with active groups and preventing reactions between them and organic compounds and lead to the production of active radicals with lower oxidation potentials such as $ClOH^{\bullet-}$, $CO_3^{\bullet-}$, $NO_3^{\bullet-}$, $NO_2^{\bullet-}$, $Cl^{\bullet}$ and

$Cl_2^{\bullet-}$ (Eqs. (10) to (17)), which leads to reduce of process efficiency [2, 48]. Also, the adsorption of anions on the catalyst surface leads to clogging of the pores of the catalyst surface the reduction of active sites, thus reducing catalyst activity in the presence of anions [2]. Compared to the inhibitory effects of anions, as shown in Fig. 6a, SO_4^{2-} has the least effect and HCO_3^- anion has the greatest inhibitory effect on the catalytic degradation of MNZ.

For HCO_3^-, there are significant inhibitory effects due to trapping $^{\bullet}OH$ and $SO_4^{\bullet-}$ radicals and the production of weak oxidizing species such as $CO3^{\bullet-}$ and $HCO3^{\bullet-}$ (E0 = 1.78 V) Eqs. (10 and 11) [2]. So, the efficiency of MNZ removal was decreased. SO_4^{2-} anions react with $^{\bullet}OH$ radicals to produce $SO_4^{\bullet-}$ weak radicals Eq. (12).

The inhibitory effect Cl^- and NO_3^- ions he oxidative elimination of MNZ can be due to their function as scavenging agents and the production of weak oxidative species such as $NO_3^{\bullet-}$ (E0 = 2.30 V), $NO_2^{\bullet-}$ (E0 = 1.03 V), $Cl^{\bullet}$ (E0 = 2.4 V) and $Cl_2^{\bullet-}$ (E0 = 2.0 V) through electron transfer reaction Eqs. (13) to (17). Also, PMS molecules are consumed by Cl^- ions in a non-radical route to generate SO_4^{2-} ions and HSO_4^- Eqs. (13) to (20) [2, 49].

$$\rightarrow SO_4^{2-} + {}^{\bullet}OH \qquad SO_4^{\bullet-} + OH^- \tag{10}$$

$$\rightarrow HCO_3^- + SO_4^{\bullet-} \qquad H + CO_3^{\bullet-} + SO_4^{2-} \tag{11}$$

$$\rightarrow HCO_3^- + {}^{\bullet}OH \qquad H_2O + CO_3^{-\bullet} \tag{12}$$

$$NO_3^- \rightarrow + \ {}^{\bullet}OH/SO_4^{\bullet-} \qquad NO_3^{\bullet} + OH^-/SO_4^{2-} \tag{13}$$

$$\rightarrow H_2O + NO_3^{\bullet} \qquad 2OH^- \ + NO_2^{\bullet} \tag{14}$$

$$\rightarrow SO_4^{\bullet-} + Cl^- \qquad Cl^{\bullet} + SO_4^{2-} \tag{15}$$

$$^{\bullet}OH \rightarrow + Cl^- \qquad ClOH^{\bullet-} \tag{16}$$

$$\rightarrow Cl^- + Cl^{\bullet} \qquad Cl_2^{\bullet-} \tag{17}$$

$$\rightarrow Cl^- + \ HSO_5^- \qquad HOCl + SO_4^{2-} \tag{18}$$

$$\rightarrow Cl^{-+} \ HSO_5^- \qquad OCl + HSO4^- \tag{19}$$

$$\rightarrow 2Cl^- + H^+ + HSO_5^- \qquad HOCl + SO_4^{2-} \tag{20}$$

Radical scavenger

Quenching testes were used to determine the role of reactive species in the removal of MNZ over $CuFe_2O_4$/GO/PMS process. In this work, tert-butanol (TBA) and ethanol (EtOH) were applied as scavengers of hydroxyl and sulfate radicals respectively under optimal conditions (0.2 g/L catalyst pH 5.0, 30 mg/L MNZ and 2 mM PMS). EtOH known as a scavenger in quenching both radicals $SO_4^{\bullet-}$ ($3.2 \times 10^6\ M^{-1}\ s^{-1}$) and $^{\bullet}OH$ ($9.7 \times 10^8\ M^{-1}\ s^{-1}$), while.

the TBA known as a specific scavenger of •OH [27]. According to Fig. 7a, that the MNZ degradation efficiency decreased by addition EtOH and TBA, Also, hydroxyl and sulfate species were involved in the degradation process in $Cufe_2o_4$/GO/PMS system. The highest and lowest suppressing effect on MNZ degradation was assigned to EtOH (80%) and TBA (63%). a Significant inhibitory effect of EtOH demonstrates that •OH and $SO4^{\bullet-}$ species show an important role in the elimination of MNZ [2]. However, Less inhibitory effects for TBA implies that the •OH species were not the major oxidizing radicals and play a small role in the degradation of MNZ by the $CuFe_2O_4$/GO/ PMS process [2]. According to these results, $SO_4^{\bullet-}$ radicals are most participation in the removal of MNZ by $CuFe_2O_4$/GO/ PMS system.

Stability, reusability and mineralization degree of catalyst

Reusing of catalytic is a parameter more cost-effective in real applications. The reusability, durability, mineralization degree of MNZ and leached the iron and copper to the solution for $CuFe_2O_4$/GO catalyst was examined for five consecutive runs under optimized conditions (0.2 g/L catalyst, pH 5.0, 2 mM PMS and 30 mg/L MNZ). in Fig. 7b, The results obtained for all studied runs showed that the leaching amounts of iron and copper to the solution in the 2nd run were 0.13 and 0.11 mg/L and reduced to 0.072 and 0.045 mg/L in the 5th run, leached amounts <0.2 mg/L in all studied runs that set by the WHO, proves the great physicochemical stability of $CuFe_2O_4$/GO [2]. MNZ removal and mineralization degree were declined from 100% in the 1st run (within 60 min reaction) to 90.4% after 5th runs, which represents the successful mineralization of metronidazole over several runs. Similar results were also reported in previous studies [2, 41]. Removal of TOC by CuFe2O4/GO/PMS system was reduced over five cycles. According to Fig. 6b, the removal efficiencies of TOC from 56.75 for first run to 41.02%in the fifth run. The reduction of efficiency during five consecutive runs can be due to clogging of the catalyst surface by MNZ molecules and reduction of available sites, as well as the production and presence of intermediaries which are more resistant to oxidizing radicals, resulting in reduced catalyst capacity [2]. In conclusion, the catalyst can have the acceptable reusability potential and e cost-effective after five consecutive runs.

PMS activation mechanisms

The reactions of PMS decomposition happen in both liquid phase (solution mixture) and solid phase (the catalyst surface). In solid phase, PMS decompositions occurs and produced species of $SO4^{\bullet-}{}_{(ads)}$ and $HO^{\bullet}{}_{(ads)}$ in surface of the catalyst, while in liquid phase produced species of $SO4^{\bullet-}{}_{(free)}$ and $HO^{\bullet}{}_{(free)}$ [27]. In the solid phase, some reactions occur between PMS

molecules and transition metals such as $Fe^{2+/}$ Fe^{3+} and $Cu^{+/}$ Cu^{2+} ions in $CuFe_2O_4$ NPs and reactive species are produced in the form of $SO_4^{\bullet-}{}_{(ads)}$ and $SO_5^{\bullet-}{}_{(ads)}$ according to Eqs. (21) to (25). Also, the decomposition of PMS by graphene oxide occurs as a result of the transfer of electrons from the catalyst surface to produce active radicals ($HO^{\bullet}{}_{(ads)}$). So, in this phase, both graphene oxide and ferrite copper are involved in the production of active species according to Eqs. (27) and (28).

In the solution phase, PMS molecules are activated by iron and copper ions leached from the catalyst, and formed $SO_4^{\bullet-}{}_{(free)}$ and $HO^{\bullet}{}_{(free)}$ radicals (Eqs. 21 to 26). Also, in these reactions, $SO_5^{\bullet-}$ species can form at the catalytic surface and in aquatic solution and have low oxidation potential (Eqs. (23 and 25)). [2] Under these electron transfer reactions, generated reactive species in both solution and solid phases can attack MNZ molecules to form MNZ $^{\bullet+}$ and H_2O to generate (OH) MNZ $^{\bullet}$ radicals. Also, (OH) MNZ $^{\bullet}$ can be produced by reaction between $HO^{\bullet}$ and MNZ. Finally, (OH) MNZ $^{\bullet}$ is decomposed to intermediates, CO_2 and H_2O during oxidation reactions, (Eqs. (26 to 30)).

$$\rightarrow\equiv Cu^{2+} + HSO_5^- \quad \equiv SO_4^{\bullet-} + Cu^+ + OH^+ \tag{21}$$

$$\rightarrow\equiv Cu^{+} + HSO_5^- \quad \equiv SO_4^{\bullet-} + Cu^{2+} + OH^- \tag{22}$$

$$\rightarrow\equiv Cu^{3+} + HSO_5^- \quad \equiv Cu^{+2} + H^+ + SO_5^{\bullet-} \tag{23}$$

$$\rightarrow\equiv Fe^{2+} + HSO_5^- \quad \equiv Fe^{3+} + OH^- + SO_4^{\bullet-} \tag{24}$$

$$\rightarrow\equiv Fe^{3+} + HSO_5^- \quad \equiv Fe^{2+} + H^+ + SO_5^{\bullet-} \tag{25}$$

$$\rightarrow SO_4^{\bullet-} + H2O \quad H^+ + SO_4^{2-} + {}^{\bullet}OH \tag{26}$$

$$\rightarrow HSO_5^- + GO \quad SO_4^{\bullet-} + OH^- + GO^+ \tag{27}$$

$$\rightarrow HSO_5^- + GO \quad SO_4^{\bullet-} + {}^{\bullet}OH + GO^+ \tag{28}$$

$$\rightarrow SO_4^{\bullet-} + MNZ \quad MNZ^{\bullet+} + SO42^- \tag{29}$$

$$\rightarrow MNZ^{\bullet+} + H2O \quad (OH)\ MNZ^{\bullet} + H^+ \tag{30}$$

$$\rightarrow {}^{\bullet}OH + MNZ \quad (OH)\ MNZ^{\bullet} \tag{31}$$

$$\rightarrow\rightarrow (OH)\ MNZ^{\bullet} \quad \text{degradation products} \quad H_2O + CO_2 \tag{32}$$

Conclusion

The $CuFe_2O_4$/GO magnetic nanocomposite was used as an environmentally friendly catalyst to activate PMS molecules to decomposition MNZ. The prepared catalyst represented an excellent activities towards PMS and generation of $SO_4^{\bullet-}$ radicals. Catalyst possesses operational stability and reusability during consecutive runs. Over $CuFe_2O_4$/GO/PMS system, $SO_4^{\bullet-}$ radicals contributed as dominant oxidizing species on MNZ degradation. $CuFe_2O_4$/GO/PMS showed very good removal efficiency in decomposition of MNZ (100%) and (%41.02) TOC Under optimal conditions, and the experimental data matched well with pseudo-first-order kinetic model. Studied effect of anions showed HCO_3^- ions the strongest hampering on the efficiency of $CuFe_2O_4$/GO/PMS system. This study presented the $CuFe_2O_4$/GO catalyst as a durable and recyclable catalyst with good ability to decompose PMS. This system showed good efficiency in refining resistant organic matter and has good potential for use in real applications.

Acknowledgments Financial support for this study is provided by 32659 project number from Iran University of Medical Sciences, Tehran, Iran.

Compliance with ethical standards

Conflict of interest The authors of this article declare that they have no conflict of interests.

References

1. Fick J, Söderström H, Lindberg RH, Phan C, Tysklind M, Larsson DJ. Contamination of surface, ground, and drinking water from pharmaceutical production. Environ Toxicol Chem. 2009;28(12): 2522–7.
2. Noroozi R, Gholami M, Farzadkia M, Jonidi Jafari A. Degradation of ciprofloxacin by CuFe2O4/GO activated PMS process in aqueous solution: performance, mechanism and degradation pathway. Int J Environ Anal Chem. 2020:1–22.
3. Khan NA, Khan SU, Ahmed S, Farooqi IH, Yousefi M, Mohammadi AA. and Changani F. Recent trends in disposal and treatment technologies of emerging-pollutants-A critical review. TrAC Trends Anal Chem. 2020;122:115744.
4. Kafaei R, Papari F, Seyedabadi M, Sahebi S, Tahmasebi R, Ahmadi M, et al. Occurrence, distribution, and potential sources of antibiotics pollution in the water-sediment of the northern coastline of the Persian Gulf. Iran Science of the Total Environment. 2018;627: 703–12.
5. Petrie B, Barden R, Kasprzyk-Hordern B. A review on emerging contaminants in wastewaters and the environment: current knowledge, understudied areas and recommendations for future monitoring. Water Res. 2015;72:3–27.
6. Azamateslamtalab E, Madani M, Ramavandi B, Mohammadi R. Sonication alkaline–assisted preparation of Rhizopus oryzae biomass for facile bio-elimination of tetracycline antibiotic from an aqueous matrix. Environ Sci Pollut Res. 2020:1–10.
7. Khan NA, Ahmed S, Farooqi IH, Ali I, Vambol V, Changani F, et al. Occurrence, sources and conventional treatment techniques for various antibiotics present in hospital wastewaters: a critical review. TrAC Trends Anal Chem. 2020;129:115921.
8. Pan Y, Li X, Fu K, Deng H, Shi J. Degradation of metronidazole by UV/chlorine treatment: efficiency, mechanism, pathways and DBPs formation. Chemosphere. 2019;224:228–36.
9. Wang X, Du Y, Ma J. Novel synthesis of carbon spheres supported nanoscale zero-valent iron for removal of metronidazole. Appl Surf Sci. 2016;390:50–9.
10. Ramavandi B, Akbarzadeh S. Removal of metronidazole antibiotic from contaminated water using a coagulant extracted from Plantago ovata. Desalin Water Treat. 2015;55(8):2221–8.

11. Fang Z, Chen J, Qiu X, Qiu X, Cheng W, Zhu L. Effective removal of antibiotic metronidazole from water by nanoscale zero-valent iron particles. Desalination. 2011;268(1–3):60–7.
12. Sepehr MN, Al-Musawi TJ, Ghahramani E, Kazemian H, Zarrabi M. Adsorption performance of magnesium/aluminum layered double hydroxide nanoparticles for metronidazole from aqueous solution. Arab J Chem. 2017;10(5):611–23.
13. Fakhravar S, Farhadian M, Tangestaninejad S. Excellent performance of a novel dual Z-scheme Cu2S/Ag2S/BiVO4 heterostructure in metronidazole degradation in batch and continuous systems: immobilization of catalytic particles on α-Al2O3 fiber. Appl Surf Sci. 2020;505:144599.
14. Azadbakht F, Esrafili A, Yeganeh Badi M, Sajedifar J, Amiri M, Gholami M. Efficiency of persulfate-based advanced oxidation process (UV/Na2S2O8) in removal of metronidazole from aqueous solutions. J Mazandaran Univ Med Sci. 2017;27(154):119–29.
15. Dai Q, Zhou J, Weng M, Luo X, Feng D, Chen J. Electrochemical oxidation metronidazole with co modified PbO2 electrode: degradation and mechanism. Sep Purif Technol. 2016;166:109–16.
16. Görmez F, Görmez Ö, Gözmen B, Kalderis D. Degradation of chloramphenicol and metronidazole by electro-Fenton process using graphene oxide-Fe3O4 as heterogeneous catalyst. J Environ Chem Eng. 2019;7(2):102990.
17. Wang Q, Cai Z, Huang L, Pan Y, Quan X, Puma GL. Intensified degradation and mineralization of antibiotic metronidazole in photo-assisted microbial fuel cells with Mo-W catalytic cathodes under anaerobic or aerobic conditions in the presence of Fe (III). Chem Eng J. 2019;376:119566.
18. Khan A, Liao Z, Liu Y, Jawad A, Ifthikar J, Chen Z. Synergistic degradation of phenols using peroxymonosulfate activated by CuO-Co3O4@ MnO2 nanocatalyst. J Hazard Mater. 2017;329:262–71.
19. Damiri F, Dobaradaran S, Hashemi S, Foroutan R, Vosoughi M, Sahebi S, et al. Waste sludge from shipping docks as a catalyst to remove amoxicillin in water with hydrogen peroxide and ultrasound. Ultrason Sonochem. 2020:105187.
20. Farhadi N, Tabatabaie T, Ramavandi B, Amiri F. Optimization and characterization of zeolite-titanate for ibuprofen elimination by sonication/hydrogen peroxide/ultraviolet activity. Ultrason Sonochem. 2020:105122.
21. Jafari AJ, Kakavandi B, Jaafarzadeh N, Kalantary RR, Ahmadi M, Babaei AA. Fenton-like catalytic oxidation of tetracycline by AC@ Fe3O4 as a heterogeneous persulfate activator: adsorption and degradation studies. J Ind Eng Chem. 2017;45:323–33.
22. Khan AH, Khan NA, Ahmed S, Dhingra A, Singh CP, Khan SU, et al. Application of advanced oxidation processes followed by different treatment technologies for hospital wastewater treatment. J Clean Prod. 2020:122411.
23. Ren Y, Lin L, Ma J, Yang J, Feng J, Fan Z. Sulfate radicals induced from peroxymonosulfate by magnetic ferrospinel MFe2O4 (M= co, cu, Mn, and Zn) as heterogeneous catalysts in the water. Appl Catal B Environ. 2015;165:572–8.
24. Deng J, Feng S, Zhang K, Li J, Wang H, Zhang T, et al. Heterogeneous activation of peroxymonosulfate using ordered mesoporous Co3O4 for the degradation of chloramphenicol at neutral pH. Chem Eng J. 2017;308:505–15.
25. Li X, Xiao B, Wu M, Wang L, Chen R, Wei Y, et al. In-situ generation of multi-homogeneous/heterogeneous Fe-based Fenton catalysts toward rapid degradation of organic pollutants at near neutral pH. Chemosphere. 2020;245:125663.
26. Li J, Li Y, Xiong Z, Yao G, Lai B. The electrochemical advanced oxidation processes coupling of oxidants for organic pollutants degradation: a mini-review. Chin Chem Lett. 2019;30(12):2139–46.
27. Khaghani R, Kakavandi B, Ghadirinejad K, Fard ED, Asadi A. Preparation, characterization and catalytic potential of γ-Fe2O3@ AC mesoporous heterojunction for activation of peroxymonosulfate into degradation of cyfluthrin insecticide. Microporous Mesoporous Mater. 2019;284:111–21.
28. Chen L, Ding D, Liu C, Cai H, Qu Y, Yang S, et al. Degradation of norfloxacin by CoFe2O4-GO composite coupled with peroxymonosulfate: a comparative study and mechanistic consideration. Chem Eng J. 2018;334:273–84.
29. Li H, Gao Q, Wang G, Han B, Xia K, Zhou C. Architecturing CoTiO3 overlayer on nanosheets-assembled hierarchical TiO2 nanospheres as a highly active and robust catalyst for peroxymonosulfate activation and metronidazole degradation. Chem Eng J. 2020;392:123819.
30. MirzaHedayat B, Noorisepehr M, Dehghanifard E, Esrafili A, Norozi R. Evaluation of photocatalytic degradation of 2, 4-Dinitrophenol from synthetic wastewater using Fe3O4@ SiO2@ TiO2/rGO magnetic nanoparticles. J Mol Liq. 2018;264:571–8.
31. Foroutan R, Mohammadi R, Ramavandi B. Elimination performance of methylene blue, methyl violet, and Nile blue from aqueous media using AC/CoFe 2 O 4 as a recyclable magnetic composite. Environ Sci Pollut Res. 2019;26(19):19523–39.
32. Foroutan R, Mohammadi R, Ramavandi B, Bastanian M. Removal characteristics of chromium by activated carbon/CoFe 2 O 4 magnetic composite and Phoenix dactylifera stone carbon. Korean J Chem Eng. 2018;35(11):2207–19.
33. Zhang T, Zhu H, Croué J-P. Production of sulfate radical from peroxymonosulfate induced by a magnetically separable CuFe2O4 spinel in water: efficiency, stability, and mechanism. Environ Sci Technol. 2013;47(6):2784–91.
34. Nirumand L, Farhadi S, Zabardasti A. Magnetically separable Ag/CuFe2O4/reduced Graphene oxide ternary Nanocomposite with high performance for the removal of Nitrophenols and dye pollutants from aqueous media. Acta Chim Slov. 2018;65(4):919–31.
35. Noroozi R, Al-Musawi TJ, Kazemian H, Kalhori EM, Zarrabi M. Removal of cyanide using surface-modified Linde type-a zeolite nanoparticles as an efficient and eco-friendly material. J Water Process Eng. 2018;21:44–51.
36. Tu Y-J, You C-F, Chen M-H, Duan Y-P. Efficient removal/recovery of Pb onto environmentally friendly fabricated copper ferrite nanoparticles. J Taiwan Inst Chem Eng. 2017;71:197–205.
37. Tang Y, Guo H, Xiao L, Yu S, Gao N, Wang Y. Synthesis of reduced graphene oxide/magnetite composites and investigation of their adsorption performance of fluoroquinolone antibiotics. Colloids Surf A Physicochem Eng Asp. 2013;424:74–80.
38. Wu L-K, Wu H, Zhang H-B, Cao H-Z, Hou G-Y, Tang Y-P, et al. Graphene oxide/CuFe2O4 foam as an efficient absorbent for arsenic removal from water. Chem Eng J. 2018;334:1808–19.
39. Sharifi S, Nabizadeh R, Akbarpour B, Azari A, Ghaffari HR, Nazmara S, et al. Modeling and optimizing parameters affecting hexavalent chromium adsorption from aqueous solutions using Ti-XAD7 nanocomposite: RSM-CCD approach, kinetic, and isotherm studies. J Environ Health Sci Eng. 2019;17(2):873–88.
40. Foroutan R, Peighambardoust SJ, Mohammadi R, Omidvar M, Sorial GA, Ramavandi B. Influence of chitosan and magnetic iron nanoparticles on chromium adsorption behavior of natural clay: adaptive neuro-fuzzy inference modeling. Int J Biol Macromol. 2020;151:355–65.
41. Zhang X, Feng M, Qu R, Liu H, Wang L, Wang Z. Catalytic degradation of diethyl phthalate in aqueous solution by persulfate activated with nano-scaled magnetic CuFe2O4/MWCNTs. Chem Eng J. 2016;301:1–11.
42. Fan J, Qin H, Jiang S. Mn-doped g-C3N4 composite to activate peroxymonosulfate for acetaminophen degradation: the role of superoxide anion and singlet oxygen. Chem Eng J. 2019;359:723–32.
43. Ammar HB, Brahim MB, Abdelhédi R, Samet Y. Enhanced degradation of metronidazole by sunlight via photo-Fenton process under gradual addition of hydrogen peroxide. J Mol Catal A Chem. 2016;420:222–7.

44. Rao Y, Qu L, Yang H, Chu W. Degradation of carbamazepine by Fe (II)-activated persulfate process. J Hazard Mater. 2014;268:23–32.
45. Hu L, Zhang G, Liu M, Wang Q, Dong S, Wang P. Application of nickel foam-supported Co3O4-Bi2O3 as a heterogeneous catalyst for BPA removal by peroxymonosulfate activation. Sci Total Environ. 2019;647:352–61.
46. Kong J, Li R, Wang F, Chen P, Liu H, Liu G, et al. Sulfate radical-induced transformation of trimethoprim with CuFe 2 O 4/ MWCNTs as a heterogeneous catalyst of peroxymonosulfate: mechanisms and reaction pathways. RSC Adv. 2018;8(44): 24787–95.
47. Deng J, Shao Y, Gao N, Tan C, Zhou S, Hu X. CoFe2O4 magnetic nanoparticles as a highly active heterogeneous catalyst of oxone for the degradation of diclofenac in water. J Hazard Mater. 2013;262: 836–44.
48. Wang Y, Tian D, Chu W, Li M, Lu X. Nanoscaled magnetic CuFe2O4 as an activator of peroxymonosulfate for the degradation of antibiotics norfloxacin. Sep Purif Technol. 2019;212:536–44.
49. Xu L, Chu W, Gan L. Environmental application of graphene-based CoFe2O4 as an activator of peroxymonosulfate for the degradation of a plasticizer. Chem Eng J. 2015;263:435–43.